

Enhanced ferromagnetism of CrI₃ bilayer by self-intercalation

Yu Guo, Nanshu Liu, Yanyan Zhao, Xue Jiang, Si Zhou,* Jijun Zhao

Key Laboratory of Materials Modification by Laser, Ion and Electron Beams, Dalian University of Technology, Ministry of Education, Dalian 116024, China

Abstract

Two-dimensional (2D) ferromagnets with high Curie temperature have long been the pursuit for electronic and spintronic applications. CrI₃ is a rising star of intrinsic 2D ferromagnets, however, it suffers from weak exchange coupling. Here we propose a general strategy of self-intercalation to achieve enhanced ferromagnetism in bilayer CrI₃. We showed that filling either Cr or I atoms into the van der Waals gap of stacked and twisted CrI₃ bilayers can induce the double exchange effect and significantly strengthen the interlayer ferromagnetic coupling. According to our first-principles calculations, the intercalated native atoms act as covalent bridge between two CrI₃ layers and lead to discrepant oxidation states for the Cr atoms. These theoretical results offer a facile route to achieve high-Curie-temperature 2D magnets for device implementation.

PACS: 75.50.Dd, 75.30.Et , 75.50.Pp

* Corresponding author. Email: sizhou@dlut.edu.cn

The discoveries of magnetism at the atomic layer limit have opened a new avenue for the research of two-dimensional (2D) materials.^[1-3] Recently, monolayer CrI₃ has been synthesized in the experiment^[4] and confirmed to be an intrinsic 2D Ising ferromagnetic (FM) material.^[5] It possesses many excellent characters, such as perfect crystalline order, strong anisotropy in magnetic configuration, and a suitable band gap of about 1.2 eV.^[6] However, the Curie temperature of monolayer CrI₃ is only 45 K due to the weak intralayer exchange,^[7] while bilayer CrI₃ with monoclinic stacking even exhibits antiferromagnetic (AFM) spin order between the two layers, which hinders the practical application of this novel 2D material.^[7] Therefore, it is highly desirable to seek effective strategies to enhance the ferromagnetism and raise the Curie temperature of 2D CrI₃.

Intercalation has also been demonstrated as a powerful approach to modulate the physical and chemical properties of 2D layered materials. So far, various atoms, ions, or molecules can be intercalated in numerous kinds of 2D materials with well controlled concentration, triggering exotic phenomena for practical applications. For instance, Li intercalation of graphene film remarkably increases optical transmittance and electrical conductivity,^[8] while Ca intercalation of bilayer graphene drives superconductivity.^[9] 2D SnS₂ intercalated by different transition metal atoms can exhibit *p*-type, *n*-type and degenerately doped semiconducting behavior.^[10] High Curie temperature up to ~300 K can be achieved in 2D magnets Fe_{3-*x*}GeTe₂ and Cr₂Ge₂Te₆ by intercalation of Na and organic ions, respectively.^[11-12] TaS₂ sheets intercalated with Fe atoms using chemical vapor transport method show tunable magnetic order, magnetic anisotropy, and magnetoresistance.^[13-15] Cl intercalation of g-C₃N₄ monolayer promotes charge carrier migration and yields favorable band gap and band edge positions to improve the photocatalytic performance for water splitting and CO₂ reduction.^[16] Furthermore, intercalation of native atoms into bilayer transition metal dichalcogenides during growth is feasible in laboratory, which allows the generation of a new class of covalently bonded materials with stoichiometry- or composition-dependent properties. For example, by controlling the metal chemical potential, a range of self-intercalated compounds of TaS(Se)₂ can be obtained, such as

Ta₉S₁₆, Ta₇S₁₂, Ta₁₀S₁₆, Ta₈Se₁₂ and Ta₉Se₁₂, some of which exhibit ferromagnetism or the unique Kagome lattice.^[17]

Motivated by recent experimental advances in the intercalated 2D materials, herein we propose a feasible strategy to elevate the Curie temperature for stacked and twisted bilayer CrI₃ by self-intercalation of Cr or I atoms. By first-principles calculations, the geometries, electronic band structures, and magnetic behavior of bilayer CrI₃ with various intercalation configurations and concentrations have been systematically investigated. The key parameters that govern the exchange energy of intercalated bilayer CrI₃ have been determined, and the underlying double exchange mechanism was elucidated.

First-principles calculations were performed using spin-polarized density functional theory in conjunction with the projector augmented wave potentials, as implemented in the VASP.^[18-19] To describe exchange-correlation interactions, we used the generalized gradient approximation with the Perdew-Burke-Ernzerhof functional.^[20] The energy cutoff for the planewave basis was chosen as 500 eV. The convergence criteria of total energy and residual force on each atom were set to be 10^{-7} eV and 0.01 eV/Å, respectively. A vacuum region of 20 Å was added to the perpendicular direction to eliminate the interaction between periodic images. Uniform **k**-point meshes with spacing of ~ 0.015 Å⁻¹ were adopted to sample the 2D Brillouin zones.

We started from the crystal structures of bilayer CrI₃ with different stacking geometries. Two types of stacked bilayer CrI₃ were considered, namely low-temperature (LT) and high-temperature (HT) phases, as shown in Fig. 1a and 1b, respectively. They have nearly identical lattice parameter (6.97 Å) and interlayer distance (3.54 Å). In order to explore the preferred magnetic interaction, we defined the exchange energy per formula (f.u.) as

$$\Delta E = (E_{\text{AFM}} - E_{\text{FM}})/n \quad (1)$$

where E_{AFM} and E_{FM} are the energies of CrI₃ bilayer with AFM and FM spin configurations between the two layers, respectively; n is the number of CrI₃ formula in the supercell. Positive (negative) value of ΔE represents FM (AFM) spin order

between the two CrI₃ layers. Larger ΔE means stronger interlayer FM coupling and generally leads to higher Curie temperature.^[21] As given in Table 1, ΔE for pristine bilayer CrI₃ are as small as 2.19 meV/f.u. (LT) and -0.14 meV/f.u. (HT), respectively, which are consistent with previous experimental observation of weak ferromagnetism in LT phase and antiferromagnetism in HT phase and close to the reported theoretical values (3.90 meV/f.u. for LT phase and -0.17 meV/f.u. for HT phase).^[4, 7, 21-24]

During the growth process, 2D layered materials with twisted angles are commonly observed in experiments,^[25-27] offering extra degree of freedom for modulating their physical properties.^[28-32] Therefore, we also considered bilayer CrI₃ with twisted angles of 21.79° and 38.42° displayed in Fig. 1 and Fig. S1 in the Supplementary Material (SM), thereafter named as 21.79°-CrI₃ and 38.42°-CrI₃, respectively. The interlayer binding energies of these twisted CrI₃ bilayers are nearly identical to that of the LT and HT phases (0.39 meV/atom), indicating favorable formation of both twisted and stacked CrI₃ sheets in the experiment. The considered twisted systems exhibit interlayer ferromagnetic coupling with smaller exchange energies than that of the LT phase, i.e. $\Delta E = 0.61$ and 0.99 meV/f.u. for 21.79°-CrI₃ and 38.42°-CrI₃, respectively. Apparently, it is difficult to enhance the ferromagnetism of bilayer CrI₃ simply by twisting the two layers, and other strategies are desired to increase the exchange energy or even change the exchange mechanism.

Inspired by successful intercalation in various layered materials,^[11-15, 17, 33-41] here we explore the possibility of self-intercalation of Cr or I atoms into bilayer CrI₃, as displayed in Fig. 1 and Fig. S1 in the SM. Starting from $\sqrt{3} \times \sqrt{3}$, 2×2 , $\sqrt{7} \times \sqrt{7}$ and 3×3 supercells of the LT and HT phases, a Cr or I atom is intercalated between CrI₃ layers, resulting in different concentrations (defined as the ratio of one Cr or I atom to the number of CrI₃ formula in the supercell). For all the systems, the intercalated Cr or I atom is always bonded with the nearby I atoms with bond lengths of around 2.79 and 2.92 Å, respectively, which are close to the intralayer Cr-I bond length of 2.77 Å. Compared with the interlayer spacing of 3.54 Å for the pristine bilayer, the intercalated Cr atom stays on the hollow site and reduces the interlayer distance to

about 3.40 Å, while the intercalated I atom locates on the bridge site of the two nearest intralayer I atoms and enlarges the interlayer spacing to up to 4.26 Å. Such difference originates from the distinct Cr–I and I–I bond nature, which is also reflected in the intercalation energies for Cr and I atoms discussed below.

To characterize the energetic stability of intercalated atoms, we define the intercalation energy as

$$E_{\text{int}} = E_{\text{tot}} - E_{\text{bilayer}} - E_{\text{Cr/I}} \quad (2)$$

where E_{tot} and E_{bilayer} are the energies of bilayer CrI_3 with and without intercalation, respectively; $E_{\text{Cr/I}}$ is the energy of a single Cr or I atom. As listed in Table S1 of SM, intercalation energies of Cr (I) atom for the LT and HT phases are in the range of $-3.97 \sim -4.11$ eV ($-0.13 \sim -0.31$ eV) and $-4.29 \sim -4.39$ eV ($-0.69 \sim -1.61$ eV), respectively. The twisted systems have E_{int} close to the values of the LT phase (about -4.00 and -0.39 eV for Cr and I intercalation, respectively). These results suggest that self-intercalation of Cr or I atoms into the vdW gap of stacked or twisted CrI_3 bilayer is energetically feasible. Compared with I intercalation, the magnitude of E_{int} for the Cr-intercalated systems is several times larger, again indicating the stronger bond formation between the intercalated Cr atom and nearest in-plane I atoms. Interestingly, the magnitudes of these intercalation energies are comparable to the formation energies of single Cr and I vacancy in the pristine CrI_3 layers (4.00 and 1.15 eV, respectively), implying that the escaped Cr and I atoms from vacancy defects may be self-intercalated into the vdW gap between CrI_3 layers. Moreover, tearing the intercalated bilayer off bulk CrI_3 involves an exfoliation energy of 0.20 J/m^2 , almost the same as that for ripping monolayer CrI_3 from the bulk material (0.21 J/m^2 , see Fig. S4 in the SM for details). Thus, self-intercalation would not affect the exfoliation behavior of layered CrI_3 . The thermal stability of intercalated CrI_3 bilayers was further assessed by the Born-Oppenheimer molecular dynamics (BOMD) simulation (see Fig. S2 in the SM). The intercalated CrI_3 bilayers can maintain their structures at 300 K for at least 10 ps simulation with the largest deviation of 0.41 Å, demonstrating their good stability at room temperature. Moreover, the diffusion behavior of the intercalated Cr atom in the vdW gap of LT and HT phases was examined (Fig. S3 in

the SM), which involves moderate barriers of 0.54 and 0.74 eV, respectively, and implies the easy migration of Cr atom to fill in the vdW gap.

Most encouragingly, self-intercalating Cr or I atoms into bilayer CrI_3 can significantly increase the exchange energy (ΔE) and elevate the Curie temperature. All the considered stacking and twisted systems become ferromagnetic order for the interlayer spin configuration. As displayed by the spin charge density in Fig. S5 in the SM, the magnetic moments are carried by both intralayer and intercalated Cr atoms. Table 1 presents ΔE values in the range of 6.78 ~ 38.58 meV/f.u. for Cr intercalation and 3.15 ~ 21.05 meV/f.u. for I intercalation, which is one or two orders of magnitude larger than the values of pristine CrI_3 bilayers (2.95 meV/f.u. for LT phase, -0.14 meV/f.u. for HT phase, 0.61 meV/f.u. for 21.79°-CrI_3 , and 0.99 meV/f.u. for 38.42°-CrI_3). Especially, the exchange energy increases linearly with the intercalated Cr concentration (Fig. 2), suggesting that the magnetism of CrI_3 bilayer can be effectively modulated by Cr intercalation. According to our previous study, the exchange energy of CrI_3 bilayer can be increased up to 9.42 meV/f.u. by proximity effect, which elevates T_c up to 130 K.^[42-43] The exchange energy is positively correlated with Curie temperature and can reflect the trend of robustness of FM order. The present self-intercalated CrI_3 bilayers with much larger exchange energies would possess even higher Curie temperature than 130 K. Similar results are also found for trilayer and bulk CrI_3 by Cr intercalation with exchange energies increased to 19.66 meV/f.u. for the LT phase (3.30 meV/f.u. for pristine systems), while AFM-to-FM transition occurs for the HT phase (see Fig. S8 and Table S3 in the SM). Therefore, self-intercalation is an effective strategy to enhance the ferromagnetism of layered CrI_3 .

The enhanced interlayer FM coupling can be understood by the decomposed charge density, electronic band structures and density of states in Fig. 3, Fig. S5, Fig. S6 and Fig. S7 in the SM. Under octahedral crystal field, the fivefold degenerate d orbitals of Cr atom split into a threefold occupied t_{2g} (d_{xy} , $d_{x^2-y^2}$ and d_{z^2}) orbital and a twofold unoccupied e_g (d_{xz} and d_{yz}) orbital. Self-intercalation induces notable electronic states in the gap that promote the hybridization between e_g and t_{2g} states,

which in turn is the key for strengthening the FM state of bilayer CrI_3 . The decomposed spin-up charge density of conduction band minimum further reveals the gradually increasing occupation of e_g orbital as the concentration of intercalated Cr atom increases. The e_g - t_{2g} coupling strength can be quantitatively characterized by the virtual exchange gap (G_{ex}) between the e_g and t_{2g} orbitals,^[44] which can be measured from the projected density of states. Taking Cr intercalation as a representative, G_{ex} values for various intercalated bilayers are in the range of 0.37 ~ 0.83 eV, remarkably smaller than the values of LT (0.98 eV) and HT (0.92 eV) phases. Generally speaking, G_{ex} decreases with increasing Cr concentration, leading to the gradually increased ΔE and enhanced ferromagnetism of bilayer CrI_3 (see Fig. 2).

To gain further insights into the impact of self-intercalation on the electronic band structure of bilayer CrI_3 , we examined the bond nature, charge transfer and oxidation states. As revealed by the electron density counter plot in Fig. 4a, the two CrI_3 layers have interlayer bonding through the intercalated Cr or I atoms. The intercalated Cr atom gains 0.02 ~ 0.12 e from the intralayer Cr atoms nearby according to Bader charge analysis in Table S5 in the SM, thereby modifying the oxidation states of Cr atoms. Taking the HT phase as a representative (see Fig. 4b), the intercalated Cr atom has a formal valence state of +2, while the two nearest intralayer Cr atoms (sharing an I atom with intercalated Cr) have a formal valence state of +2.67, compared with +3 for Cr in pristine CrI_3 bilayer. The presence of intercalated and intralayer Cr atoms with different oxidation states signifies the double exchange mechanism^[45-46] that dominates the interlayer ferromagnetism in CrI_3 bilayer, as illustrated by Fig. 4c. In the $\text{Cr}^{\delta+}\text{-Cr}^{2+}$ ($2 < \delta < 3$) mixed valence complexes, an electron hops between $\text{Cr}^{\delta+}$ and Cr^{3+} cations through a bridging I^- anion. Within the double exchange picture, electron transfer from one Cr cation to another would be more easily if it does not have to flip spin orientation in order to conform with Hund's rule, which thus facilitates the ferromagnetic coupling between two Cr cations with different valences. Similar double exchange mechanism is also applicable to bilayer CrI_3 with I intercalation (see Fig. S9). Even though the intercalated I atom is not spin-polarized, it donates certain amounts of electrons (0.06

$\sim 0.11 e$) to the adjacent I atoms in the two CrI_3 layers, which in turn leads to different valence states for the nearby intralayer Cr atoms.

In summary, we significantly enhance the interlayer ferromagnetic order of bilayer CrI_3 by self-intercalation of Cr or I atoms. The magnetic behavior of intercalated bilayer CrI_3 of the LT and HT stacking geometries or with a twisted angle has been systematically explored as a function of intercalated concentration. Both Cr and I intercalation lead to robust interlayer ferromagnetic order for all the considered CrI_3 bilayers. The exchange energy increases with the intercalated Cr concentration, reaching about 40 meV/f.u. compared to the values of pristine CrI_3 bilayer (2.95 meV/f.u. for LT phase and -0.14 meV/f.u. for HT phase). Such strong ferromagnetism is dominated by the double exchange mechanism originated from the interlayer charge transfer via the intercalated atoms, which results in different oxidation states for the Cr atoms in CrI_3 bilayers and enhanced e_g - t_{2g} hybridization. These theoretical results provide a universal and experimentally feasible strategy to effectively raise the Curie temperature of 2D ferromagnets via self-intercalation for practical uses.

Acknowledgement

This work was supported by the China Postdoctoral Science Foundation (BX20190052, 2020M670739), the National Natural Science Foundation of China (11974068), and the Fundamental Research Funds for the Central Universities of China (DUT20LAB110). The authors acknowledge the computer resources provided by the Supercomputing Center of Dalian University of Technology and Shanghai Supercomputer Center.

References

- [1] Geim A K, Grigorieva I V *Nature* 2013 499 419.
- [2] Wang Q H, Kalantar-Zadeh K, Kis A, Coleman J N, Strano M S *Nat. Nanotechnol.* 2012 7 699.
- [3] Fivaz R, Mooser E *Phys. Rev.* 1967 163 743.
- [4] Huang B, Clark G, Navarro-Moratalla E, Klein D R, Cheng R, Seyler K L, Zhong D, Schmidgall E, McGuire M A, Cobden D H *Nature* 2017 546 270.
- [5] Niu B, Su T, Francisco B A, Ghosh S, Kargar F, Huang X, Lohmann M, Li J, Xu Y, Taniguchi T *Nano Lett.* 2019 20 553.
- [6] Wang H, Fan F, Zhu S, Wu H *EPL (Europhysics Letters)* 2016 114 47001.
- [7] Huang B, Clark G, Klein D R, MacNeill D, Navarro-Moratalla E, Seyler K L, Wilson N, McGuire M A, Cobden D H, Xiao D *Nat. Nanotechnol.* 2018 13 544.
- [8] Bao W, Wan J, Han X, Cai X, Zhu H, Kim D, Ma D, Xu Y, Munday J N, Drew H D *Nat. Commun.* 2014 5 4224.
- [9] Ichinokura S, Sugawara K, Takayama A, Takahashi T, Hasegawa S *Acs Nano* 2016 10 2761.
- [10] Gong Y, Yuan H, Wu C-L, Tang P, Yang S-Z, Yang A, Li G, Liu B, van de Groep J, Brongersma M L, Chisholm M F, Zhang S-C, Zhou W, Cui Y *Nat. Nanotechnol.* 2018 13 294.
- [11] Wang N, Tang H, Shi M, Zhang H, Zhuo W, Liu D, Meng F, Ma L, Ying J, Zou L *J. Am. Chem. Soc.* 2019 141 17166.
- [12] Weber D, Trout A H, McComb D W, Goldberger J E *Nano Lett.* 2019 19 5031.
- [13] Zhang C, Yuan Y, Wang M, Li P, Zhang J, Wen Y, Zhou S, Zhang X-X *Phys. Rev. Mater.* 2019 3 114403.
- [14] Hardy W J, Chen C-W, Marcinkova A, Ji H, Sinova J, Natelson D, Morosan E *Phys. Rev. B* 2015 91 054426.
- [15] Morosan E, Zandbergen H, Li L, Lee M, Checkelsky J, Heinrich M, Siegrist T, Ong N P, Cava R J *Phys. Rev. B* 2007 75 104401.
- [16] Liu C, Zhang Y, Dong F, Reshak A, Ye L, Pinna N, Zeng C, Zhang T, Huang H *Appl. Catal. B-Environ.* 2017 203 465.
- [17] Zhao X, Song P, Wang C, Riis-Jensen A C, Fu W, Deng Y, Wan D, Kang L, Ning S, Dan J *Nature* 2020 581 171.
- [18] Kresse G, Furthmüller J *Phys. Rev. B* 1996 54 11169.
- [19] Kresse G, Joubert D *Phys. Rev. B* 1999 59 1758.
- [20] Perdew J P, Burke K, Ernzerhof M *Phys. Rev. Lett.* 1996 77 3865.
- [21] Sivadas N, Okamoto S, Xu X, Fennie C J, Xiao D *Nano Lett.* 2018 18 7658.
- [22] Klein D R, MacNeill D, Lado J L, Soriano D, Navarro-Moratalla E, Watanabe K, Taniguchi T, Manni S, Canfield P, Fernández-Rossier J *Science* 2018 360 1218.
- [23] Song T, Cai X, Tu M W-Y, Zhang X, Huang B, Wilson N P, Seyler K L, Zhu L,

- Taniguchi T, Watanabe K *Science* 2018 360 1214.
- [24] Morell E S, León A, Miwa R H, Vargas P *2D Mater.* 2019 6 025020.
- [25] Cao Y, Fatemi V, Fang S, Watanabe K, Taniguchi T, Kaxiras E, Jarillo-Herrero P *Nature* 2018 556 43.
- [26] Cao Y, Chowdhury D, Rodan-Legrain D, Rubies-Bigorda O, Watanabe K, Taniguchi T, Senthil T, Jarillo-Herrero P *Phys. Rev. Lett.* 2020 124 076801.
- [27] Cao Y, Fatemi V, Demir A, Fang S, Tomarken S L, Luo J Y, Sanchez-Yamagishi J D, Watanabe K, Taniguchi T, Kaxiras E *Nature* 2018 556 80.
- [28] Yan W, He W-Y, Chu Z-D, Liu M, Meng L, Dou R-F, Zhang Y, Liu Z, Nie J-C, He L *Nat. Commun.* 2013 4 2159.
- [29] Yin L-J, Qiao J-B, Zuo W-J, Li W-T, He L *Phys. Rev. B* 2015 92 081406.
- [30] Fang T, Liu T, Jiang Z, Yang R, Servati P, Xia G *ACS Applied Nano Materials* 2019 2 3138.
- [31] Lim H E, Miyata Y, Kitaura R, Nishimura Y, Nishimoto Y, Irle S, Warner J H, Kataura H, Shinohara H *Nat. Commun.* 2013 4 2548.
- [32] Liu N, Zhang J, Zhou S, Zhao J *J. Mater. Chem. C* 2020 8 6264.
- [33] Ganguli S C, Singh H, Roy I, Bagwe V, Bala D, Thamizhavel A, Raychaudhuri P *Phys. Rev. B* 2016 93 144503.
- [34] Bointon T H, Khrapach I, Yakimova R, Shytov A V, Craciun M F, Russo S *Nano Lett.* 2014 14 1751.
- [35] Seel J, Dahn J *J. Electrochem. Soc.* 2000 147 892.
- [36] Voiry D, Yamaguchi H, Li J, Silva R, Alves D C, Fujita T, Chen M, Asefa T, Shenoy V B, Eda G *Nat. Mater.* 2013 12 850.
- [37] Koski K J, Wessells C D, Reed B W, Cha J J, Kong D, Cui Y *J. Am. Chem. Soc.* 2012 134 13773.
- [38] Yuan H, Wang H, Cui Y *Accounts Chem. Res.* 2015 48 81.
- [39] Motter J P, Koski K J, Cui Y *Chem. Mat.* 2014 26 2313.
- [40] Kovtyukhova N I, Wang Y, Lv R, Terrones M, Crespi V H, Mallouk T E *J. Am. Chem. Soc.* 2013 135 8372.
- [41] Lai H, He R, Xu X, Shi T, Wan X, Meng H, Chen K, Zhou Y, Chen Q, Liu P *Nanoscale* 2020 12 1448.
- [42] Liu N, Zhou S, Zhao J *Phys. Rev. Mater.* 2020 4 094003.
- [43] Li H, Xu Y-K, Lai K, Zhang W-B *Phys. Chem. Chem. Phys.* 2019 21 11949.
- [44] Huang C, Feng J, Wu F, Ahmed D, Huang B, Xiang H, Deng K, Kan E *J. Am. Chem. Soc.* 2018 140 11519.
- [45] Goodenough J B *Phys. Rev.* 1955 100 564.
- [46] Zener C *Phys. Rev.* 1951 81 440.

Table 1. Exchange energy ΔE (in the unit of meV/f.u.) of pristine, Cr and I intercalated CrI_3 bilayers, including HT and LT phases, twisted bilayers 21.79°-CrI_3 and 38.42°-CrI_3 . The numbers in the brackets are the exchange energy for 21.79°-CrI_3 and 38.42°-CrI_3 without intercalation.

	ΔE	pristine	$\sqrt{3}\times\sqrt{3}$	2×2	$\sqrt{7}\times\sqrt{7}$	3×3	21.79°	38.42°
Cr intercalation	LT	2.95	38.58	31.48	21.33	6.78	5.38	13.17
	HT	-0.14	29.99	28.50	18.18	15.02	(0.61)	(0.99)
I intercalation	LT	2.95	6.64	6.44	3.15	18.64	3.67	6.30
	HT	-0.14	21.05	16.50	6.31	18.23		

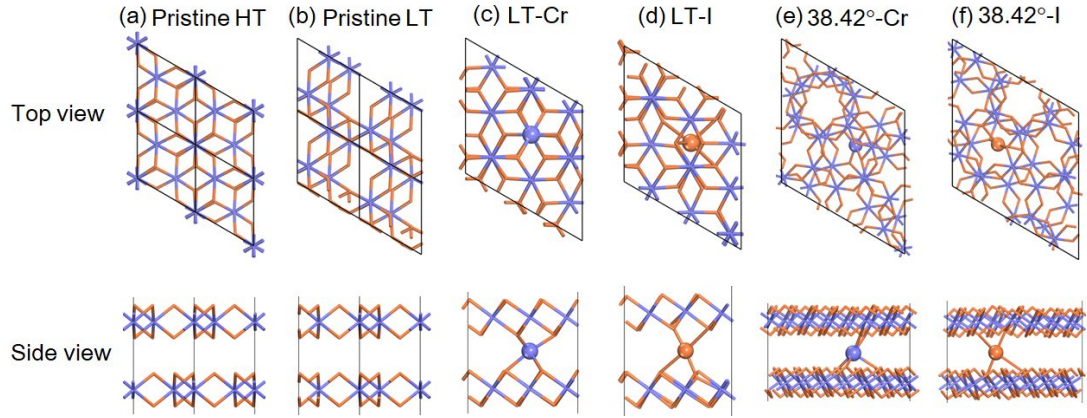


Fig. 1. Atomic structures of pristine (a) LT and (b) HT phases of bilayer CrI_3 , (c) Cr and (d) I intercalated LT phase of $\sqrt{3} \times \sqrt{3}$ supercell, and (e) Cr and (f) I intercalated twisted 38.42° - CrI_3 . The Cr and I atoms are shown in purple and orange colors, respectively.

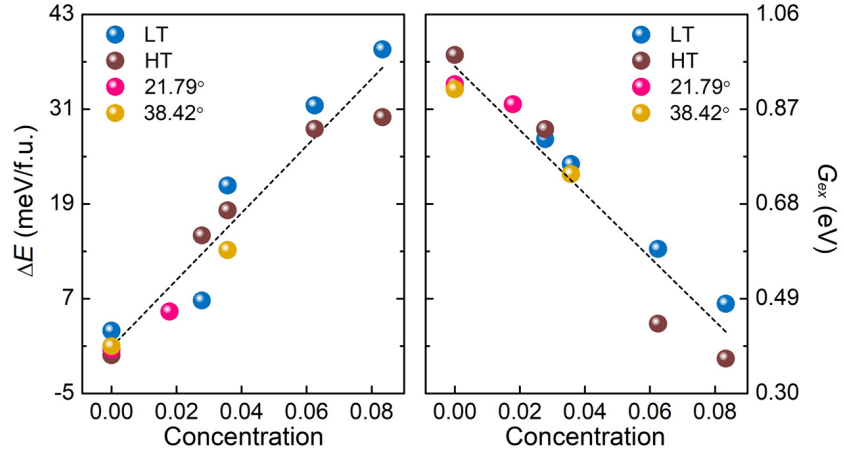


Fig. 2. Exchange energy (ΔE) and virtual exchange gap (G_{ex}) of various Cr-intercalated CrI_3 bilayers as a function of Cr intercalation concentration.

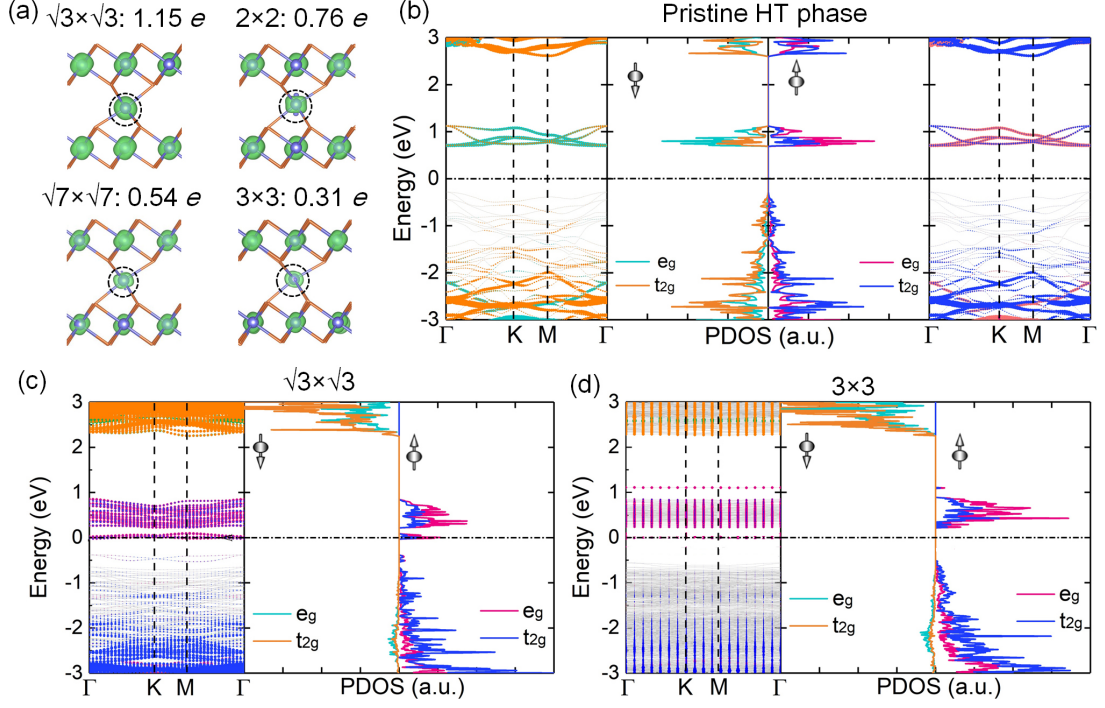


Fig. 3. (a) Decomposed spin-up charge density of conduction band minimum for Cr-intercalated bilayers in $\sqrt{3}\times\sqrt{3}$, 2×2 , $\sqrt{7}\times\sqrt{7}$ and 3×3 supercell, respectively. The isosurface value is $0.05\text{ e}/\text{\AA}^3$. The charge values at the intercalated Cr atom are present. (b-d) Band structures and project density of states (PDOS) of pristine HT phase of CrI_3 bilayer, Cr-intercalated HT phase in $\sqrt{3}\times\sqrt{3}$ and 3×3 supercell, respectively.

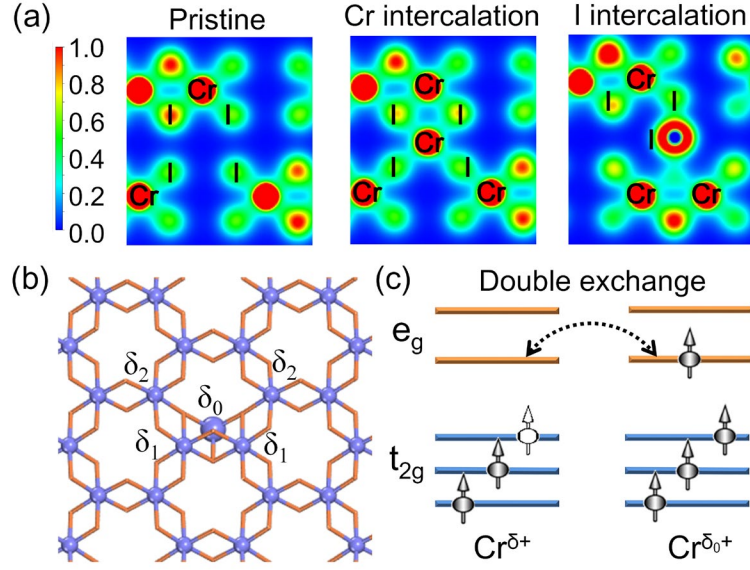


Fig. 4. (a) Contour plots for the electron densities of pristine, Cr-intercalated and I-intercalated HT phase of CrI₃ bilayer from left to right panels. (b) One layer of Cr-intercalated HT phase with the formal valence state δ_0 (+2) for intercalated Cr atom, δ_1 (+8/3) and δ_2 (+17/6) for intralayer Cr atoms, and the valence state of other unmarked Cr atoms is +3, i.e., $2 = \delta_0 < \delta_1 < \delta_2 < 3$. (c) Schematic diagram of the double exchange mechanism for Cr/I-intercalated CrI₃ bilayer. The hollow arrow indicates that the electron is not fully occupied for the orbital.

Supplementary Material

Enhanced ferromagnetism of CrI₃ bilayer by self-intercalation

Yu Guo, Nanshu Liu, Yanyan Zhao, Xue Jiang, Si Zhou, * Jijun Zhao

*Key Laboratory of Materials Modification by Laser, Ion and Electron Beams, Dalian University of
Technology, Ministry of Education, Dalian 116024, China*

* Corresponding author. Email: sizhou@dlut.edu.cn

S1. Atomic structures of intercalated CrI_3 bilayers

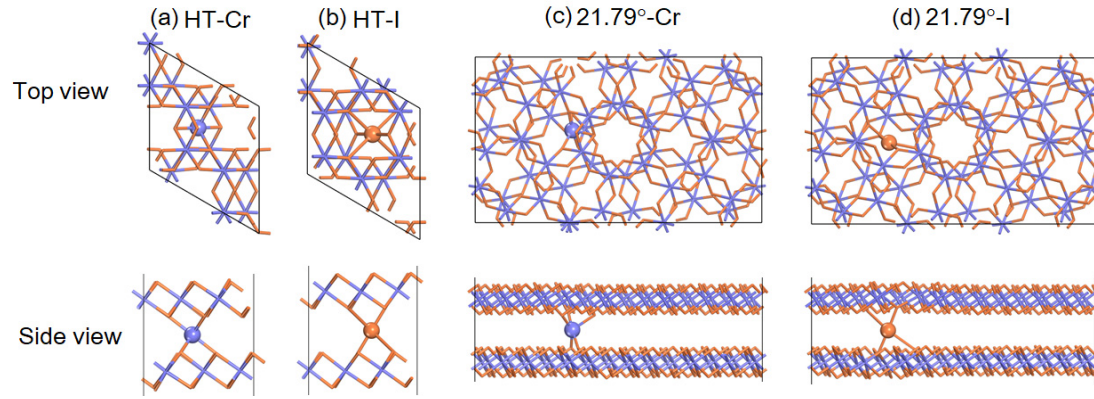


Fig. S1. Atomic structures of (a) Cr and (b) I intercalated HT phase of $\sqrt{3} \times \sqrt{3}$ supercell, and (c) Cr and (d) I intercalated twisted 21.79°- CrI_3 . The Cr and I atoms are shown in purple and orange colors, respectively.

S2. The intercalation energy for intercalated bilayers

Table S1. Intercalation energy (E_{int}) for Cr and I intercalated CrI_3 bilayers in the LT and HT phases using different supercells as well as twisted bilayers.

	E_{int} (eV)	$\sqrt{3}\times\sqrt{3}$	2×2	$\sqrt{7}\times\sqrt{7}$	3×3	21.79°	38.42°
Cr intercalation	LT	-4.01	-4.04	-4.11	-3.97	-4.23	-3.97
	HT	-4.29	-4.30	-4.35	-4.39		
I intercalation	LT	-0.18	-0.13	-0.21	-0.31	-0.37	-0.41
	HT	-0.69	-0.75	-1.23	-1.61		

S3. The interlayer distance for intercalated bilayer

Table S2. Interlayer distance for Cr and I intercalated CrI_3 bilayers in the LT and HT phases using different supercells as well as twisted bilayers. The numbers in the brackets are the exchange energies for twisted 21.79°-CrI_3 and 38.42°-CrI_3 without intercalation.

	phase	pristine	$\sqrt{3}\times\sqrt{3}$	2×2	$\sqrt{7}\times\sqrt{7}$	3×3	21.79°	38.42°
Cr intercalation	LT	3.54	3.38	3.40	3.39	3.34	3.48	3.40
	HT	3.54	3.34	3.36	3.37	3.37	(3.64)	(3.60)
I intercalation	LT	3.54	4.04	3.86	3.58	3.50	3.70	3.78
	HT	3.54	4.26	3.87	3.59	3.52		

S4. Thermodynamical stability of intercalated CrI_3 bilayers

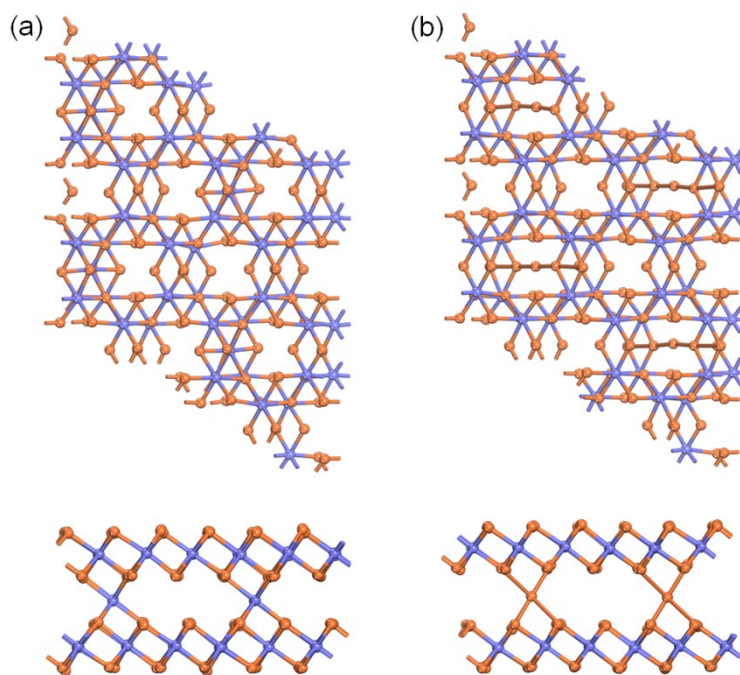


Fig. S2. Snapshots of (a) Cr and (b) I intercalated CrI_3 bilayers for HT phase from BOMD

simulations with temperature controlled at 300 K. Each simulation is lasted for 10 ps.

S5. Diffusion of intercalated Cr atom at van der Waals gap

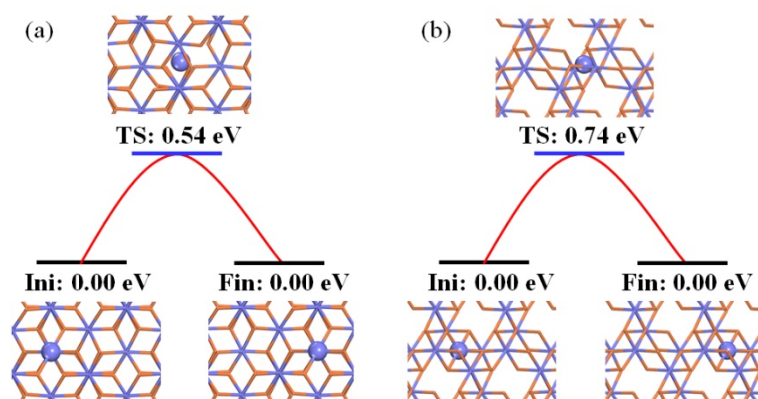


Fig. S3. Diffusion behavior of intercalated Cr atom in the van der Waals gap of (a) LT and (b) HT phases of bilayer CrI₃. The Cr and I atoms are shown in purple and orange colors, respectively. The intercalated Cr atoms are given in larger purple balls. The climbing-image nudged elastic band (CI-NEB) method was employed to investigate the diffusion kinetics and determine the activation energy for migration. Five images were used to calculate the diffusion path. The intermediate images of each CI-NEB simulation were relaxed until the perpendicular forces were smaller than 0.02 eV/Å.

S6. Exfoliation behaviors of intercalated CrI_3 systems

We calculated the exfoliation energies of intercalated and pristine CrI_3 systems by simulating the separation of one CrI_3 layer from the intercalated and pristine bilayers. The equilibrium distance between intercalated bilayer and separated layer is 3.50 Å, which can be determined by the function of distance respect to total energy (Fig. S4a). Then we simulated the exfoliation process and predicted the exfoliation energy with respect to the separation distance, as shown in Fig. S4b. The calculated exfoliation energies are 0.21 J/m^2 for pristine systems and 0.20 J/m^2 for intercalated systems, respectively, indicating that the intercalated systems preserve the exfoliation behavior of pristine layered CrI_3 .

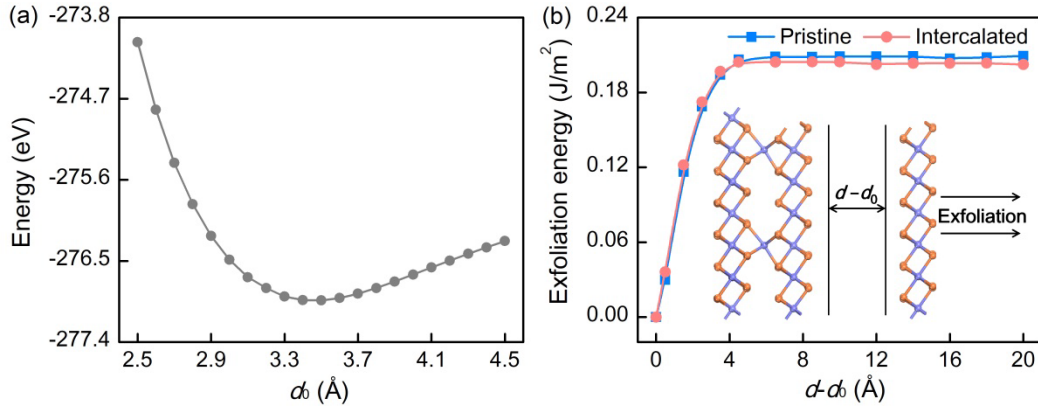


Fig. S4. (a) Total energy vs. the distance (d_0) between intercalated bilayer and a separated layer. (b) Exfoliation energy vs. separation distance d . for intercalated CrI_3 bilayer in comparison with pristine CrI_3 system..

S7. Electronic structures of intercalated bilayers

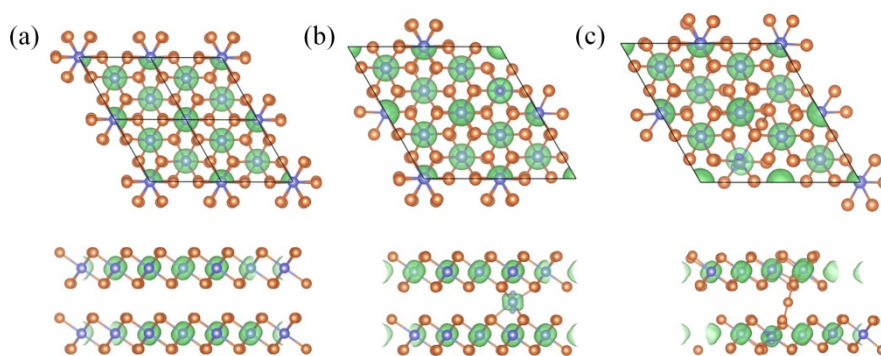


Fig. S5. Spin charge density (in green color) with an isosurface value of $0.01 \text{ e}/\text{\AA}^3$ for (a) pristine, (b) Cr and (c) I intercalated CrI_3 bilayers, respectively. The Cr and I atoms are shown in purple and orange colors, respectively.

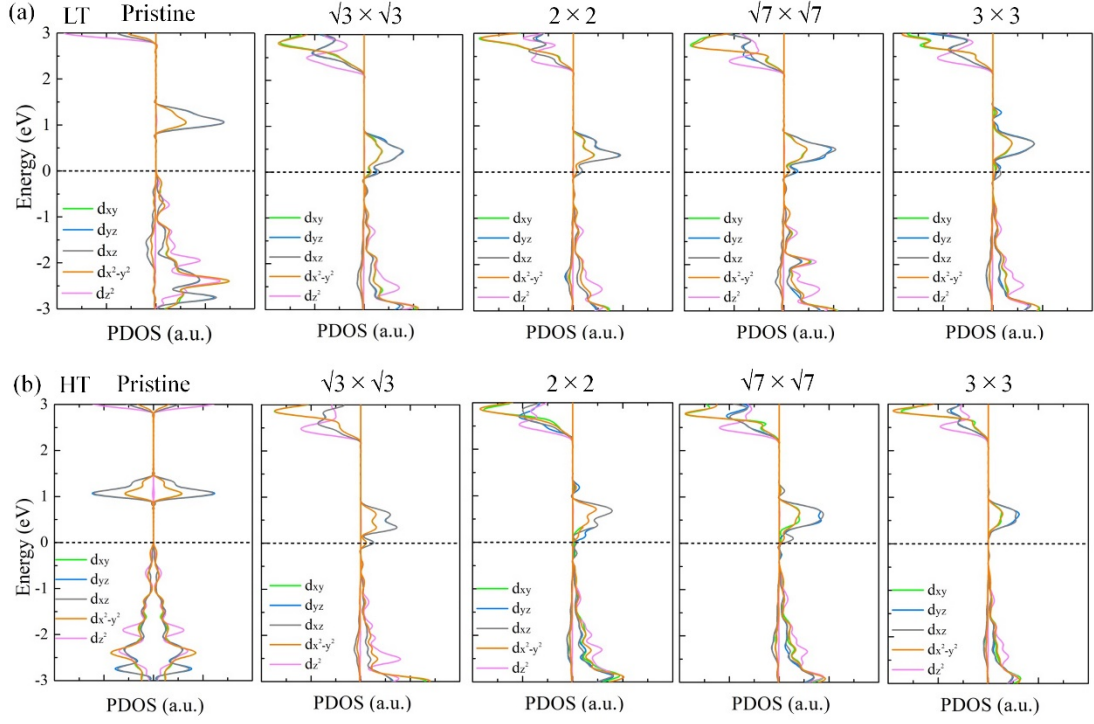


Fig. S6. Projected density of states (PDOS) of pristine and Cr-intercalated CrI_3 bilayers of (a) LT and (b) HT phases, with different supercells.

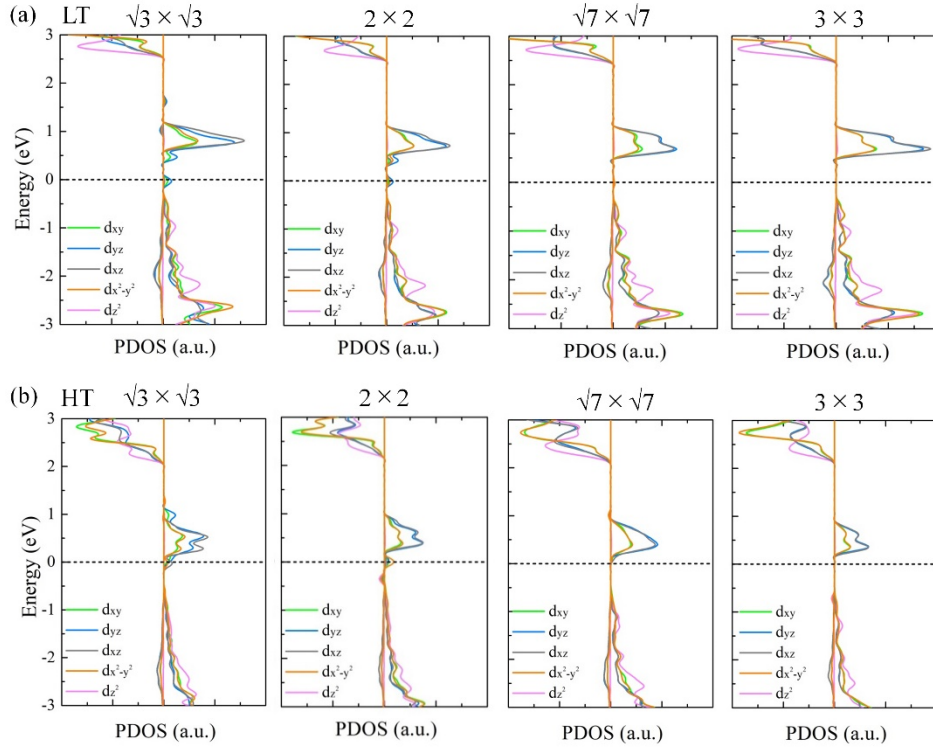


Fig. S7. Projected density of states (PDOS) of pristine and I-intercalated CrI₃ bilayers of (a) LT and (b) HT phases, with different supercells.

S8. Self-intercalation for trilayer and bulk CrI_3

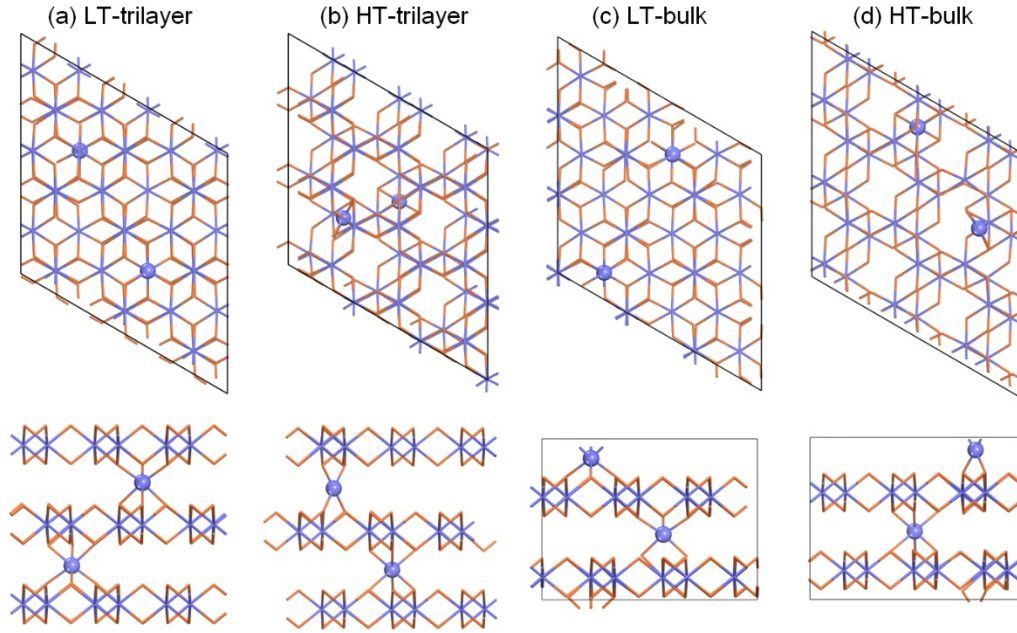


Fig. S8. Atomic structures of Cr intercalated (a) (c) LT and (b) (d) HT phases for trilayer and bulk CrI_3 in 3×3 supercell.

Table S3. Exchange energy ΔE of pristine, trilayer and bulk in LT and HT phases of 3×3 supercell. The atomic structures are shown in Fig. S8.

ΔE (meV/f.u.)	Trilayer		Bulk	
	Pristine	Intercalated	Pristine	Intercalated
LT	2.03	7.01	3.30	19.66
HT	-0.20	6.34	-0.98	13.15

S9. Virtual exchange gap for intercalated CrI₃ bilayers

Table S4. Virtual exchange gap (G_{ex}) of Cr-intercalated bilayer CrI₃ of the LT and HT phases with different supercells.

G_{ex} (eV)	pristine	$\sqrt{3}\times\sqrt{3}$	2×2	$\sqrt{7}\times\sqrt{7}$	3×3
LT	0.98	0.37	0.44	0.74	0.83
HT	0.92	0.48	0.59	0.76	0.81

S10. Charge transfer for the intercalated CrI₃ bilayers

Table S5. Charge transfer (CT, in the unit of electrons) of Cr and I-intercalated bilayer CrI₃ of the LT and HT phases with different supercells.

	CT (<i>e</i>)	$\sqrt{3}\times\sqrt{3}$	2×2	$\sqrt{7}\times\sqrt{7}$	3×3
Cr intercalation	LT	0.11	0.06	0.04	0.02
	HT	0.11	0.12	0.11	0.12
I intercalation	LT	0.08	0.06	0.07	0.06
	HT	0.10	0.06	0.11	0.11

S11. Double exchange for I-intercalated bilayers

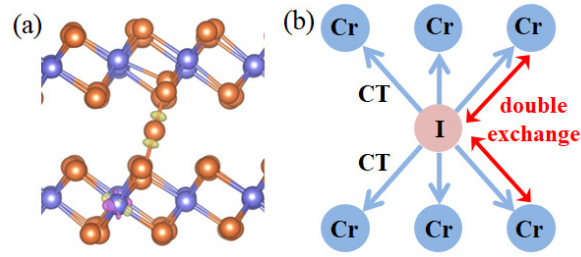


Fig. S9. Differential charge density of (a) I-intercalated LT phase of bilayer CrI₃. Yellow and pink colors represent the charge accumulation and depletion regions, respectively, with an isosurface value of $8 \times 10^{-3} e/\text{\AA}^3$. (b) Schematic illustrations of double exchange in the I-intercalated CrI₃ bilayer. Blue arrows show the charge transfer (CT) from the intercalated I atom to the intralayer Cr atoms, and red arrows highlight the double exchange interaction between Cr-Cr atoms.